PCCP

ROYAL SOCIETY OF CHEMISTRY

PAPER

View Article Online
View Journal

Cite this: DOI: 10.1039/d6cp00698a

Resolving the trifecta of discrepancies regarding the phosphorus suboxide P_4O

Ethan J. Poncelet, [ab] Alexander G. Heide, [a] Mitchell E. Lahm, [a] Henry F. Schaefer III [a] and Yohannes Abate *[b]

Unsatisfied with vibrational and mechanistic discrepancies between three previous investigations, we characterized the P_4O potential energy surface with high-level coupled cluster methods for resolution, up to CCSD(T)/cc-pV(T+d)Z. Our computations substantiate the previous vibrational band assignments of Andrews and coworkers to cyclic and terminal P_4O. The antisymmetric P–O stretch of bridge-bonded P_4O was previously assigned to a band at 856 cm^{-1}, and the symmetric stretch was assigned to a lower frequency band at 553 cm^{-1}. In contrast, we find the symmetric P–O stretch of bridge-bonded P_4O to lie higher than the antisymmetric, and formally assign the symmetric stretch to a previously unassigned 770 cm^{-1} band. Tentative assignments for the now-elusive antisymmetric P–O stretch of bridge-bonded P_4O are discussed herein. To resolve mechanistic discrepancies, we demonstrate that the isomerization pathway between terminal and bridge-bonded P_4O is a two-step process, requiring passage through a local-minimum intermediate on the potential energy surface. It was previously suggested that the antisymmetric P–O stretch band originally assigned to bridge-bonded P_4O (856 cm^{-1}) could instead belong to a D_{2d}-symmetry P_4O_2 species, but our computed fundamental vibrational frequency (654 cm^{-1}) does not support this suggestion. New insight has revealed our previous substantiation of the vibrational band assigned to cyclic P_4O_2 to be incorrect, and we now assign the positive combination antisymmetric P–O stretch to an unassigned 919 cm^{-1} band. Focal point analysis with basis sets up to cc-pV(Q+d)Z and correlation treatment to CCSDT(Q) is performed with the addition of zero-point vibrational energies for cyclic (−95.5 kcal mol^{-1}), bridge-bonded (−92.5), and terminal P_4O (−81.7) relative to tetrahedral P_4 plus ^3P oxygen as well as D_{2d}-symmetry P_4O_2 (−62.0) relative to tetrahedral P_4 plus $^3\Sigma_g^-$ O_2. We provide the energy of $\frac{1}{2}\left[^3\Sigma_g^- O_2\right] \rightarrow {}^3P$ oxygen (+58.6 kcal mol^{-1}) using our methods for comparison to previously reported P_4O_2 species with optimal error cancellation.

Received 25th February 2026,
Accepted 1st May 2026

DOI: 10.1039/d6cp00698a

rsc.li/pccp

1. Introduction

The recent discovery of phosphorus allotropes as exfoliable van der Waals (vdW) materials has resurged interest in phosphorus oxidation chemistry due to these materials being unstable in ambient conditions.[1–10] Light, heat, water, and oxygen all influence the degradation of phosphorus materials. Visible wavelengths of light contain sufficient energy to split white phosphorus ($P_4 \rightarrow 2P_2$),[11,12] as well as instigate reactions of black and violet phosphorus films with oxygen by exciting them above their bandgaps.[1,13] Excess heat will inevitably reorder any phosphorus allotrope into amorphous, red phosphorus in the absence of contaminants. Reactions of water with phosphorus oxides are generally established, and produce various phosphorus acids. Oxidation of phosphorus in excess oxygen produces phosphorus pentoxide, which can exist as P_4O_{10} adamantane-like molecules in the gas-phase or repeating P_2O_5 subunits in the condensed-phase. Intermediate phosphorus oxides involved in the formation of P_4O_{10} remain elusive despite extensive investigation.[12,14–30]

Andrews was the first to investigate the lower oxides of phosphorus in white phosphorus (P_4) oxidation reactions in a series of articles,[12,20–24,26] the first published in 1988.[12] Therein, Andrews and Withnall reacted P_4 molecules with oxygen atoms from photolysis of ozone and microwave discharge of molecular oxygen in low-temperature argon matrices. White phosphorus is known to be quite volatile, but surprisingly, the P_4 and O_3 molecules were not reactive upon codeposition. Andrews and Withnall observed broadening and small shifts of the P_4 and O_3 fundamentals, indicating formation of P_4–O_3 complexes but no further reaction. They instigated

[a] Center for Computational Quantum Chemistry, University of Georgia, Athens, Georgia 30602, USA
[b] Department of Physics and Astronomy, University of Georgia, Athens, Georgia 30602, USA. E-mail: yohannes.abate@uga.edu; Tel: +1 706-542-2485

reactions *via* 520–1000 nm photolysis, which produced PO, PO_2, and P_4O species. Reactions were spontaneous between P_4 and oxygen atoms from microwave discharge of O_2, and the aforementioned species were also formed along with number of other phosphorus oxides.[12]

Following their identification in 1988,[12] P_4O species were investigated theoretically by Lohr in 1990[31] at the suggestion of Andrews. Lohr characterized three minima, cyclic (C-), bridge-bonded (B-), and terminal (T-)P_4O (see Section 3.1 Geometries). Of these, T- and B-P_4O were identified by Andrews and Withnall in 1988,[12] and C-P_4O was identified by Mielke, McCluskey, and Andrews in 1990.[22] Hatree–Fock (HF) with a 6-31G* basis set was used by Lohr to optimize the geometries and compute vibrational frequencies of the P_4O isomers. Good agreement was found between theoretical vibrational frequencies and those measured by Andrews and coworkers for C- and T-P_4O; however, Lohr was unable to validate the identity of the bands assigned to B-P_4O. Andrews and Withnall assigned vibrational bands at 856 and 553 cm^{-1} to the antisymmetric and symmetric P–O stretches of B-P_4O.[12] Lohr found the symmetric stretch to have a higher frequency (836 cm^{-1}) than the antisymmetric (734 cm^{-1}), which resulted from a more constrained P–O–P angle than initially thought by Andrews and Withnall. Lohr did not compute isotopic frequencies, but the disagreement between the ^{16}O frequencies cast doubt on the previous experimental assignment. Lohr suggested the possibility that a D_{2d}-symmetry P_4O_2 molecule could be responsible for the bands assigned to B-$_4$O.[31]

In 2023, Yao and coworkers provided theoretical predictions for the reactions $P_4 + O_2$ and $P_4O + O_2$ using the B3LYP/6-311++G** method.[32] They did not report symmetries for the vibrational modes, but their two highest frequency vibrations of B-P_4O (presumably the symmetric and antisymmetric P–O stretches) were predicted to be 705 and 629 cm^{-1}. These results appear to support previous theoretical predictions,[31] that the experimentally observed B-P_4O bands likely belong to a different species[12]; however, there remains a difference of over 100 cm^{-1} between the two theoretical predictions for the location of the B-P_4O vibrational bands.[31,32] Additionally, the first theoretical study found a singular transition state along the potential energy surface (PES) between T- and B-P_4O with a barrier of 13 kcal mol^{-1},[31] whereas the second predicted two transition states (2 and 3 kcal mol^{-1} barriers) with an intermediate along the PES from T- to B-P_4O.[32] Simply, the mechanistic discrepancy in the literature is whether the reaction from T- to B-P_4O proceeds through a P_3–PO intermediate or a direct insertion of the oxygen atom into the P–P bond.[31,32]

All considered, there currently exists a trifecta[12,31,32] of discrepancies regarding P_4O species. The experimental assignments for the antisymmetric and symmetric stretches of B-P_4O do not agree with the two theoretically predicted band locations. The two theoretical predictions for where these vibrational bands should lie do not agree with one another, nor whether this molecule was present in the previous experiments. Lastly, the two theoretical mechanisms for the isomerization reaction between T- and B-P_4O do not agree with each other. These discrepancies are resolved herein.

2. Methods

Geometries and harmonic vibrational frequencies were computed using the coupled cluster singles, doubles, and perturbative triples wavefunctions [CCSD(T)][33] with the correlation consistent polarized valence triple-ζ basis set including tight d-type functions on phosphorus atoms [cc-pV(T+d)Z].[34–39] Second order vibrational perturbation theory (VPT2)[40,41] was used to compute anharmonicity using the B3LYP-D3BJ/cc-pV(T+d)Z method.[42–45] Fundamental frequencies reported are thus CCSD(T)/cc-pV(T+d)Z harmonic plus δB3LYP-D3BJ/cc-pV(T+d)Z anharmonic frequencies.[46–51] Isotopic (^{18}O) harmonic vibrational frequencies were also computed, and the fundamental isotopic vibrational frequencies reported are a product of the ^{16}O fundamental frequency with a ratio of the harmonic frequencies $\left[\nu^{^{18}O}_{CCSD(T)}/\nu^{^{16}O}_{CCSD(T)}\right]$. For Hartree–Fock (HF) and correlation up to CCSD(T), single point energies were computed with the cc-pV(X+d)Z [X = D, T, Q] basis sets. Energies were extrapolated to near the complete basis set limit using focal point analysis[52–55] with additional CCSDT(Q)/cc-pV(D+d)Z single point and CCSD(T)/cc-pV(T+d)Z zero-point vibrational energy corrections.[33,56,57] DLPNO-CCSDT and DLPNO-CCSDT(Q) was utilized for P_4O_2,[58–60] while canonical full T and (Q) was used for the P_4O species.[56,57] MOLPRO 2022.1 was used to optimize geometries and compute harmonic vibrational frequencies.[61–63] ORCA 6.1 was used to obtain effects of anharmonicity, locate transition states *via* the nudged elastic band code, and for intrinsic reaction coordinate computations.[64–68] Psi4 1.10 was used for DLPNO-CCSDT and -(Q) computations.[58–60,69] MRCC 2022 was used for canonical CCSDT and -(Q) computations.[70,71]

3. Results and discussion

3.1. Geometries

In a recent article regarding P_4O_2 species,[72] we reported a systematic underestimation of antisymmetric P–O vibrational frequencies relative to experiment using the CCSD(T)/cc-pV(T+d)Z method. This behavior was unexpected, as both HF and post-HF methods typically overestimate vibrational frequencies. Additionally, experimental vibrational frequencies are typically redshifted *ca.* 10 cm^{-1} or more when measured in an argon matrix,[73,74] which was utilized by Andrews and coworkers.[12,22] We initially suggested that a methodological overestimation of P–O bond lengths may be responsible, since increased bond lengths correspond to lower vibrational frequencies. We are now more confident that this is the case. The computational gold standard, CCSD(T) with a triple-ζ polarization quality basis set, does not precisely reproduce the experimental geometry of the phosphorus monoxide radical diatomic (PO) as desired for accurate computation of vibrational frequencies. Experimentally, the equilibrium P–O bond length is 1.476 Å,[75] whereas the CCSD(T)/cc-pVTZ value is 1.495 Å. Inclusion of tight d-functions on phosphorus [cc-pV(T+d)Z] improves agreement and yields 1.487 Å, but remains 0.011 Å short. Correlation of all electrons except the phosphorus 1s

Table 1 Effect of basis set and correlation of core electrons on the P–O bond length of phosphorus monoxide. FC denotes frozen core and AE denotes correlation of all electrons (exluding the 1s core of phosphorus atoms). $\Delta^{QZ}_{r(P-O)}$ shows the difference in bond length between quadruple-ζ and triple-ζ computations, and $\Delta^{core}_{r(P-O)}$ shows the difference in bond length between AE and FC computations. Bond lengths are in angstrom

Experimental phosphorus monoxide bond length [r(P–O)] = 1.476				
Method	r(P–O)	Method	r(P–O)	$\Delta^{QZ}_{r(P-O)}$
CCSD(T)-FC/cc-pwCVTZ	1.483	CCSD(T)-FC/cc-pwCVQZ	1.480	−0.03
CCSD(T)-AE/cc-pwCVTZ	1.480	CCSD(T)-AE/cc-pwCVQZ	1.476	−0.04
$\Delta^{core}_{r(P-O)}$	−0.003		−0.004	

core with the cc-pwCVQZ basis set achieves 0.001 Å accuracy relative to experiment for the phosphorus monoxide bond length. It appears the overestimation is both due to the incompleteness of the triple-ζ basis set and not correlating the core electrons (Table 1), each affecting the bond length by a similar amount. We also tested this hypothesis on P_2O species, where again an overestimation was observed. For linear P_2O, CCSD(T)-AE/cc-pwCVQZ gave a P–O bond length of 1.466 Å and CCSD(T)/cc-pV(T+d)Z yielded 1.476 Å. For bridged P_2O, CCSD(T)-AE/cc-pwCVQZ gave a P–O bond length of 1.736 Å and CCSD(T)/cc-pV(T+d)Z yielded 1.747 Å. The CCSD(T)-AE/cc-pwCVQZ method is computationally infeasible for the system at hand; however, the systematic 0.01 Å overestimation of P–O bond lengths and accompanying underestimation of P–O vibrational frequencies should be expected for the computationally-feasible CCSD(T)/cc-pV(T+d)Z method.

Fig. 1 contains the CCSD(T)/cc-pV(T+d)Z optimized geometries of C-P_4O, B-P_4O, T-P_4O, and D_{2d}-symmetry P_4O_2. C-P_4O is a planar, C_{2v} ring in which the P–O–P motif at the apex is connected *via* single bonds. Double P=P bonds lie on the edges of the C-P_4O ring, whereas the phosphorus atoms at the base are connected *via* a single P–P bond. C-P_4O shares little resemblance with the P_4 tetrahedron, and has been predicted to be formed from the reaction of $P_2O + P_2$.[22] B- and T-P_4O closely resemble the P_4 tetrahedron, and have been predicted to be formed from the reaction $P_4 + O$.[12] B-P_4O (C_{2v}) also contains a P–O–P motif akin to C-P_4O, but each of the phosphorus atoms in the P–O–P motif of B-P_4O are connected to both of the phosphorus atoms at the base *via* single P–P bonds. T-P_4O features a double P=O bond at the apex of a trigonal pyramid of singly-bonded phosphorus atoms. The D_{2d}-symmetry P_4O_2 structure resembles the adamantane-backbone analogue, P_4O_6, where four of the bridge-bonded oxygen atoms are replaced with P–P bonds.

As mentioned, we previously observed an underestimation of P–O–P vibrational frequencies in P_4O_2 species, which stemmed from the overestimation of P–O bond lengths in P–O–P motifs. Considering the difference between the P–O bond lengths in C-P_4O (1.649 Å), B-P_4O (1.692), and D_{2d}-symmetry P_4O_2 (1.696), it is simply not possible to precisely anticipate the P–O bond lengths in phosphorus suboxides. Nevertheless, we could expect our CCSD(T)/cc-pV(T+d)Z method to overestimate P–O bond lengths *ca.* 0.01 Å, as shown for the smaller phosphorus oxides.

The following discussion is of the computed CCSD(T)/cc-pV(T+d)Z optimized geometries, and the previously mentioned inconsistencies with experiment should be kept in mind. Recent gas-phase electron diffraction data by Wu and co-workers yielded 2.199 Å P–P bond lengths for the white phosphorus tetrahedron.[76] Double P=P bonds in C-P_4O have a length of 2.064 Å, and the single P–P bond has a length of 2.166 Å. Longer than the single bonds in both C-P_4O and P_4, the single P–P bonds of B-P_4O have lengths of 2.239 Å (base–base) and 2.248 Å (base–apex). P–P bonds in T-P_4O dramatically vary in length, as the edges of the trigonal pyramid have lengths of 2.134 Å and the base has lengths of 2.300 Å. We attribute this feature to the electronegative oxygen atom pulling electron density from the phosphorus atom at the apex, which in turn draws the base closer to the apex and causes a large lengthening of the basal P–P bonds. D_{2d}-symmetry P_4O_2 has similarly elongated P–P bonds, with lengths of 2.315 Å.

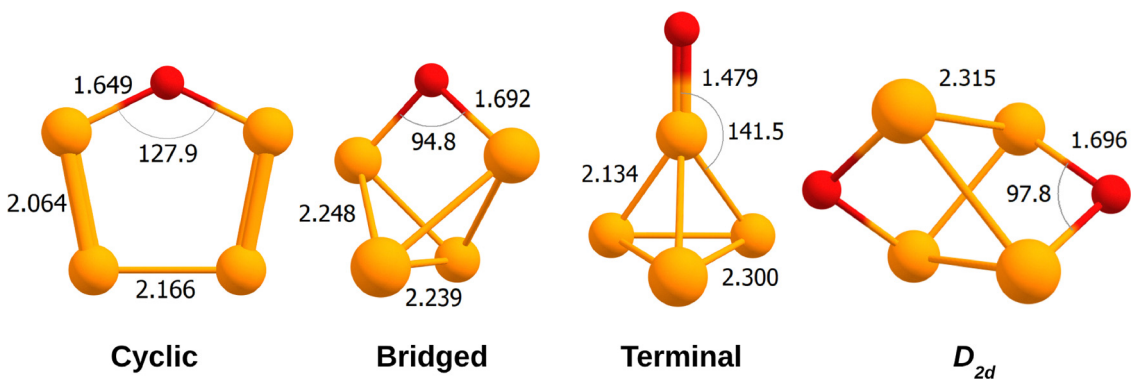

Fig. 1 CCSD(T)/cc-pV(T+d)Z geometries of cyclic P_4O (C_{2v}), bridge-bonded P_4O (C_{2v}), terminal P_4O (C_{3v}), and D_{2d}-symmetry P_4O_2 are depicted.

3.2. Vibrational frequencies

One vibrational band was previously assigned to C-P_4O by Andrews and Mielke in their matrix isolation experiment reacting P_2 with O_3 in argon.[22] This C-P_4O band was located at 826 cm^{-1} (redshifted 36 cm^{-1} with ^{18}O) and was assigned to the b_2 P–O stretching mode. We compute a fundamental frequency of 787 cm^{-1} with a reasonable intensity (33 km mol^{-1}) and an isotopic shift of 35 cm^{-1} (Table 2). As discussed previously, our computed value lies untypically lower than the experimental value; however, we are now able to attribute this feature to the overestimation of the P–O bond lengths in P–O–P motifs by the CCSD(T)/cc-pV(T+d)Z method. In order to demonstrate, we shortened the P–O bond lengths of the C-P_4O structure by 0.01 Å, consistent our observed degree of overestimation, and computed harmonic CCSD(T)/cc-pV(T+d)Z vibrational frequencies from the modified, non-stationary C-P_4O geometry. Others have demonstrated the effectiveness of similar approaches.[77,78] The computed b_2 P–O fundamental vibrational frequency from our adjusted geometry was 823 cm^{-1}, which compares much better to the 826 cm^{-1} value obtained experimentally by Andrews and Mielke. To further demonstrate the rationality of this approach, the non-stationary harmonic frequencies were also computed in the normal mode basis of the equilibrium geometry using the CMA1-B method.[79–81] All off diagonal elements were included, and we found maximum total energy distribution (TED)[82–84] coupling to be 0.2% (1 cm^{-1}).

An unassigned 676 cm^{-1} band observed in the same experiment could appear to be the a_1 P–O stretch mode of C-P_4O since it has a reasonable intensity of 34 km mol^{-1} and our computed frequency for this vibration is 651 cm^{-1}. However, the 676 cm^{-1} band increases upon annealing and is absent after photolysis, whereas the 826 cm^{-1} band decreases upon annealing and increases after photolysis. Additionally, our computed isotopic shift is 17 cm^{-1} compared to the 29 cm^{-1} shift observed by Andrews and Mielke. These characteristics indicate the 826 and 676 cm^{-1} bands do not belong to the same molecular species.

There is a concerning discrepancy between our predicted a_1 and b_2 P–O stretching frequencies of B-P_4O and those assigned experimentally (Table 3). Andrews and coworkers assigned an 856 cm^{-1} band to the b_2 P–O stretching mode of B-P_4O and a 553 cm^{-1} band to its symmetric counterpart.[12] Understandably, Andrews and coworkers concluded that these bands belonged to the P–O stretching modes of B-P_4O because they lie *ca.* 100 cm^{-1} below the P–O stretching modes of P_4O_6, and B-P_4O would have a more constrained P–O–P angle. Lohr was the first to report theoretical vibrational frequencies for B-P_4O,[31] where he found the energetic ordering of the symmetric and antisymmetric P–O stretching modes (respectively 836 and 734 cm^{-1}) to be opposite of the assignments by Andrews and coworkers. Similar to Lohr, we predict the a_1 P–O stretching mode to lie higher than the b_2 (respectively 740 and 642 cm^{-1}); however, our predicted vibrational frequencies are much lower than those predicted by Lohr due to the severe underestimation of P–O bond lengths by HF theory. As we did for C-P_4O, we reduced the P–O bond lengths of B-P_4O by 0.01 Å and computed harmonic CCSD(T)/cc-pV(T+d)Z vibrational frequencies from the adjusted non-stationary geometry. After the addition of the stationary B3LYP-D3BJ/cc-pV(T+d)Z anharmonicity, the fundamental frequencies for the symmetric and antisymmetric P–O stretches of the adjusted geometry were 758 and 664 cm^{-1}, respectively. We again verified this approach with CMA1-B,[79–81] obtaining a TED[82–84] coupling of 0.1% (1 cm^{-1}). Even after the adjustment, our computed frequencies for B-P_4O are still not in agreement with the assignments of Andrews and coworkers.[12]

In an attempt to remedy our discrepancy, we have systematically performed a series of geometry optimizations followed by vibrational frequency computations to reveal their dependence on the level of theory (Table 4). As mentioned, HF severely underestimates the P–O bond length (1.653 Å) compared to all other levels of theory, which in turn heftily raises its predicted a_1 P–O vibrational frequency (845 cm^{-1}). CCSD(T)/cc-pV(T+d)Z predicts P–O bond lengths of 1.692 Å and a vibrational frequency of 747 cm^{-1}. B3LYP compares exceptionally well to CCSD(T) with the same basis set in this case, with P–O bond lengths of 1.692 Å and a vibrational frequency of 739 cm^{-1}. Increasing the cardinality of the basis set by one [cc-pV(Q+d)Z] with the CCSD(T) wavefunction predictably shortens P–O bond lengths (1.688 Å), in turn slightly raising the vibrational frequency (750 cm^{-1}); while augmentation [aug-cc-pV(T+d)Z] predictably lengthens P–O bond lengths (1.696 Å), and slightly lowers the vibrational frequency (736 cm^{-1}).

Table 2 Composite fundamental vibrational frequencies and isotopic shifts in cm^{-1} and harmonic IR intensities in km mol^{-1} for cyclic P_4O

Cyclic P_4O (C_{2v})			
^{16}O Freq.	Int.	^{18}O Freq.	Sym.
201	0	201	a_2
298	3	287	b_1
299	1	299	b_2
432	8	423	a_1
459	9	458	a_1
537	3	537	a_1
561	9	561	b_2
651	34	634	a_1
787 (826)[a]	33	752 (790)[a]	b_2

[a] Ref. 22, experiment of Mielke, McCluskey, and Andrews[22]

Table 3 Composite fundamental vibrational frequencies and isotopic shifts in cm^{-1} and harmonic IR intensities in km mol^{-1} for bridge-bonded P_4O

Bridge-bonded P_4O (C_{2v})			
^{16}O Freq.	Int.	^{18}O Freq.	Sym.
316	4	304	b_1
327	<1	325	a_1
332	0	332	a_2
414	3	414	b_1
426	2	423	a_1
443	9	443	b_2
551	5	550	a_1
642	30	617	b_2
740 (770)[a]	58	712 (742)[a]	a_1

[a] Ref. 21, experiment of Andrews and Mielke; originally assigned 856 and 822 cm^{-1} (ref. 21)

Table 4 Geometric parameters (bond lengths in Å and angles in degrees) and antisymmetric P–O–P harmonic vibrational frequencies (in cm^{-1}) for bridge-bonded P_4O at nine selected levels of theory. Results obtained at the level of theory used throughout this investigation are in bold [CCSD(T)/cc-pV(T+d)Z]

Bridge-bonded P_4O (C_{2v})			
Level of theory	r_{P-O}	θ_{P-O-P}	ω_e
HF/cc-pV(T+d)Z	1.653	97.6	845
B3LYP-D3BJ/cc-pV(T+d)Z	1.692	95.3	739
MP2/cc-pV(T+d)Z	1.694	93.0	742
CCSD/cc-pV(T+d)Z	1.682	95.5	773
CCSD(T)/cc-pV(T+d)Z	1.692	94.8	747
CCSD(T)-X2C/cc-pV(T+d)Z	1.692	94.8	745
CCSD(T)/aug-cc-pV(T+d)Z	1.696	94.9	736
CCSD(T)/cc-pV(Q+d)Z	1.688	94.7	750
CCSD(T)-AE/cc-pwCVTZ	1.685	94.8	751

Inclusion of relativistic effects [exact two component (X2C)][85,86] at the CCSD(T)/cc-pV(T+d)Z level of theory does not have a reportable impact on the geometry, and lowers the vibrational frequency a mere 2 cm^{-1}. Correlation of all electrons, excluding the 1s of phosphorus atoms, in the CCSD(T) wavefunction and use of the appropriate polarized weighted core basis set [cc-pwCVTZ] shortens the P–O bond lengths (1.685 Å) and raises the vibrational frequency (751 cm^{-1}). These observations agree with the previous findings that increasing the cardinality of basis set (triple-ζ → quadruple-ζ) and correlation of core electrons decreases P–O bond lengths *ca.* 0.01 Å. All considered, we believe the bands originally assigned to B-P_4O by Andrews and coworkers belong to a different molecular species; however, we do not agree with the claim of Lohr[31] that B-P_4O is not evidenced in the experiments of Andrews and coworkers.[12,21]

Andrews and Mielke left vibrational bands at 830, 802, and 770 cm^{-1} unassigned, and assigned bands at 687 (P_4O_3), 668 (P_4O_4), 641 (P_4O_6), 634 (P_4O_7), and 592 cm^{-1} (P_2-$OPOPO_2$) in their $P_4 + O_3$ experiment.[21] Considering our adjusted fundamental frequency of 758 cm^{-1} and an identical isotopic shift to Andrews and Mielke (28 cm^{-1}), we believe the unassigned 770 cm^{-1} band belongs the a_1 P–O vibrational frequency of B-P_4O and not the originally assigned 553 cm^{-1} band. This 770 cm^{-1} band can also be seen in the original $P_4 + O_3$ experiment[12] and the P_4O_6 decomposition experiment.[21] We are less confident in the correct assignment for the b_2 vibrational mode of B-P_4O, as there are a number of candidate bands in the region. The isotopic shift, or lack thereof, of the 687 cm^{-1} band would take it out of contention. The 668 cm^{-1} band assigned to P_4O_4 had an isotopic shift of 39 cm^{-1}, which is quite different from our computed shift of 25 cm^{-1}. Further experiments or more advanced theoretical methods are required to identify the exact location of the b_2 mode of B-P_4O, but we believe it should lie *ca.* 650–700 cm^{-1} and not around the original 553 cm^{-1} assignment.

Our T-P_4O fundamental vibrational frequencies compare well to the experiments of Andrews and Withnall,[12] with the exception of the vibrational modes containing basal P–P stretching character (Table 5). Similar to the overestimation of P–O bond lengths in P–O–P motifs by CCSD(T)/cc-pV(T+d)Z, we believe the basal P–P bonds of T-P_4O are also overestimated. The phosphorus diatomic experimental P═P bond length is 1.893 Å, while the CCSD(T)/cc-pV(T+d)Z length is 1.910 Å. The white phosphorus tetrahedron has experimental P–P bond lengths of 2.199 Å, while the CCSD(T)/cc-PV(T+d)Z length is 2.208 Å. Therefore, in the simplest cases of double P═P and single P–P bonds, CCSD(T)/cc-pV(T+d)Z overestimates the lengths by 0.017 and 0.008 Å, respectively. We do not have enough evidence to perform a systematic adjustment of the base P–P bond lengths of T-P_4O for the most accurate computation of vibrational frequencies as we did for P–O bond lengths in P–O–P motifs of C- and B-P_4O; nevertheless, we believe the vibrational assignments of Andrews and Withnall are correct in their entirety for T-P_4O, as did Lohr.

Table 5 Composite fundamental vibrational frequencies and isotopic shifts in cm^{-1} and harmonic IR intensities in km mol^{-1} for terminally-bonded P_4O

Terminally-bonded P_4O (C_{3v})			
^{16}O Freq.	Int.	^{18}O Freq.	Sym.
247 (243)[a]	10	240 (237)[a]	e
321 (393)[a]	1	321 (393)[a]	e
396 (441)[a]	<1	391 (441)[a]	a_1
494 (501)[a]	6	494 (501)[a]	e
555 (603)[a]	<1	550 (603)[a]	a_1
1259 (1241)[a]	143	1218 (1202)[a]	a_1

[a] Ref 12, experiment of Andrews and Withnall.[12]

Lohr[31] suggested a D_{2d}-symmetry P_4O_2 species could be responsible for the 856 cm^{-1} vibrational band originally assigned to B-P_4O by Andrews and Withnall[12] due to the antisymmetric P–O stretches transforming as the degenerate e representation. We compute the e-symmetry antisymmetric P–O stretch to be 654 cm^{-1} at the CCSD(T)/cc-pV(T+d)Z level of theory (Table 6). After reducing the P–O bond lengths 0.01 Å, we find it to be 676 cm^{-1}. The negative (b_2) and positive (a_1) combinations of symmetric P–O stretches were respectively 730 and 724 cm^{-1} pre-adjustment and 746 and 741 cm^{-1} post-adjustment. We find no evidence for the formation of this D_{2d}-symmetry P_4O_2 molecule in the experiments of Andrews and coworkers;[12,21,22] nevertheless, it is a minimum on the PES and Yao predicted it to be formed from the reaction $P_4 + O_2$.[32]

Table 6 Composite fundamental vibrational frequencies and isotopic shifts in cm^{-1} and harmonic IR intensities in km mol^{-1} for D_{2d}-symmetry P_4O_2

D_{2d}-symmetry P_4O_2			
^{16}O Freq.	Int.	^{18}O Freq.	Sym.
233	2	224	e
348	0	344	a_1
354	0	354	b_1
399	2	398	e
422	1	419	b_2
505	0	501	a_1
654	23	629	e
724	0	696	a_1
730	91	702	b_2

An erroneous substantiation of a vibrational band assigned to cyclic-P_4O_2 was likely to have been made by us in a recent article.[72] Andrews and coworkers assigned a 867 cm^{-1} vibration to the positive combination antisymmetric P–O stretch vibration of cyclic-P_4O_2,[22] and we computed a fundamental frequency of 893 cm^{-1}. Their observed isotopic shift for this band was 37 cm^{-1}, and we computed a shift of 38 cm^{-1}. Considering how CCSD(T)/cc-pV(T+d)Z has continued to overestimate bridged P–O bond lengths, we reduced the P–O bond length of cyclic-P_4O_2 0.01 Å and computed harmonic CCSD(T)/cc-pV(T+d)Z frequencies. After applying the anharmonic correction, we find the adjusted vibrational frequency to be 924 cm^{-1}. Bands at 919 and 937 cm^{-1} went unassigned and had respective isotopic shifts of 40 and 37 cm^{-1}. We think either of these bands could be responsible for the cyclic-P_4O_2 positive combination antisymmetric P–O stretch vibration instead of the previously assigned 867 cm^{-1} band. The 919 cm^{-1} band lies closer to our now adjusted vibrational frequency, but the isotopic shift of the 937 cm^{-1} band lies closer to that which we compute. Considering the great agreement between the 919 cm^{-1} band and our adjusted vibrational frequency (924 cm^{-1}), we believe it is a better assignment for the cyclic-P_4O_2 species and not the originally assigned 867 cm^{-1} band. We also will not discount the possibility of the 937 cm^{-1} band, but further experimental work is required for absolute verification.

3.3. Terminal to bridge-bonded P_4O reaction coordinate

Yao and coworkers recently reported that the T- to B-P_4O isomerization reaction proceeds through an intermediate minimum on the potential energy surface,[32] while Lohr appears to have found only the second transition state (TS2).[31] Substantiating the prediction of Yao and coworkers, we also found a T- to B-P_4O isomerization reaction that proceeds through an intermediate (IM). Fig. 2 contains CCSD/cc-pV(T+d)Z optimized stationary points along the reaction coordinate (included in the SI) with CCSD(T)/cc-pV(T+d)Z single point energies. CCSD/cc-pV(T+d)Z hessian analysis was performed on the stationary points to verify that saddle points contained one imaginary vibrational frequency and that the minima only featured real vibrational modes. Intrinsic reaction coordinate computations using CCSD/cc-pV(T+d)Z were also undertaken to connect the saddle points to the minima *via* steepest descent along the potential energy surface. We found no evidence for a direct isomerization reaction, containing only one saddle point, between T- and B-P_4O.

3.4. Energetics

Focal point analysis[52–55] was used to extrapolate the energies of C-, B-, and T-P_4O relative to tetrahedral P_4 plus ^3P oxygen (Tables 7–9). HF is found to be wholly inadequate for accurate prediction of energetics for all three P_4O isomers, as the respective δMP2/cc-pV(Q+d)Z values for C-, B-, and T-P_4O are −45.89, −48.82, and −59.23 kcal mol^{-1}. MP2 performs better for C- and B-P_4O than for T-P_4O, with respective δCCSD extrapolated values of +5.62 and +7.47 kcal mol^{-1} for C- and B-P_4O and +13.81 kcal mol^{-1} for T-P_4O. As typical, CCSD(T) predicts lower energies than CCSD, and extrapolated δCCSD(T) values for C-, B-, and T-P_4O are −4.90, −3.61, and −5.55 kcal mol^{-1}. Inclusion of perturbative quadruple excitations [CCSDT(Q)] with the cc-pV(D+d)Z basis set has a larger effect on the energies than what is desirable for our purpose, considering the computational rigor. CCSDT(Q)/cc-pV(D+d)Z corrections for C-, B-, and T-P_4O are −0.78, −0.28, and −0.64 kcal mol^{-1}.

Similarly, focal point analysis was also used to extrapolate the energy of the D_{2d}-symmetry P_4O_2 species (−62.0 kcal mol^{-1}) relative to tetrahedral P_4 plus $^3\Sigma_g^-$ O_2 (Table 10). Behaving similarly to the previously investigated P_4O_2 species, δMP2 raises its energy *ca.* 20 kcal mol^{-1}, but δCCSD lowers it by

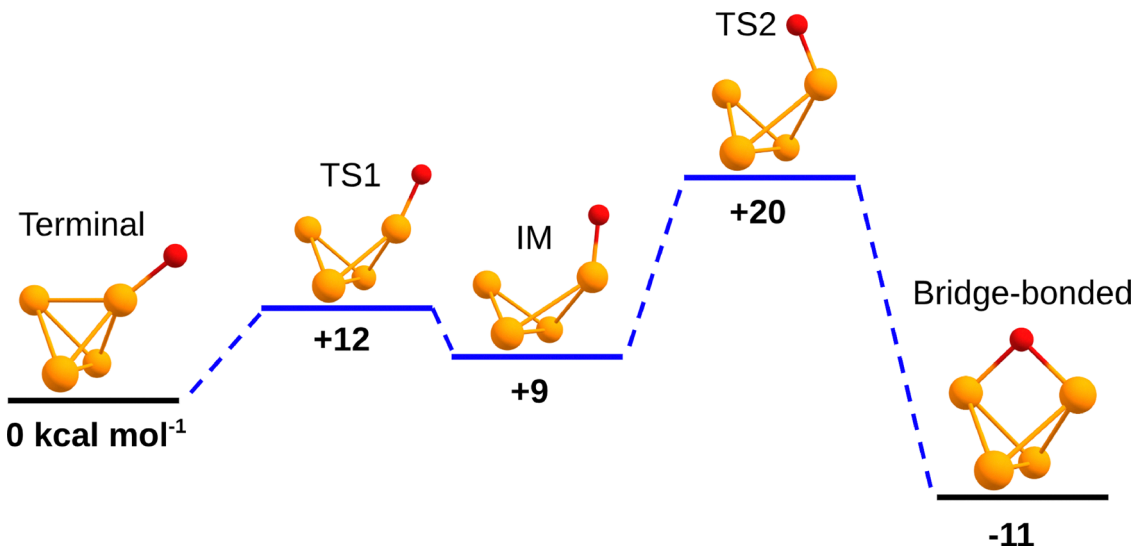

Fig. 2 CCSD(T)/cc-pV(T+d)Z//CCSD/cc-pV(T+d)Z stationary points along the T-P_4O → B-P_4O reaction coordinate. TS denotes transition state and IM denotes intermediate.

Table 7 Incremented focal point energies in kcal mol^{-1} for cyclic P_4O. Total energies are relative to tetrahedral P_4 plus ^{3}P oxygen and are reported as Net/Extrapolation + ΔZPVE

Cyclic P_4O							
Total = −97.66 + 2.18 = −95.5 kcal mol^{-1}							
	ΔHF	+δ MP2	+δ CCSD	+δ CCSD(T)	+δ CCSDT	+δ CCSDT(Q)	Net
cc-pV(D+d)Z	−38.52	−46.34	+6.19	−4.11	−0.21	−0.78	[−83.76]
cc-pV(T+d)Z	−48.05	−44.58	+5.58	−4.83	[−0.21]	[−0.78]	[−92.87]
cc-pV(Q+d)Z	−50.03	−45.89	+5.60	−4.87	[−0.21]	[−0.78]	[−96.18]
Extrapolation	[−50.53]	[−46.85]	[+5.62]	[−4.90]	[−0.21]	[−0.78]	[−97.66]

Table 8 Incremented focal point energies in kcal mol^{-1} for bridge-bonded P_4O. Total energies are relative to tetrahedral P_4 plus ^{3}P oxygen and are reported as Net/Extrapolation + ΔZPVE

Bridge-bonded P_4O							
Total = −94.65 + 2.14 = −92.5 kcal mol^{-1}							
	ΔHF	+δ MP2	+δ CCSD	+δ CCSD(T)	+δ CCSDT	+δ CCSDT(Q)	Net
cc-pV(D+d)Z	−32.75	−40.99	+5.67	−2.23	−0.21	−0.28	[−70.79]
cc-pV(T+d)Z	−45.61	−46.08	+7.17	−3.27	[−0.21]	[−0.28]	[−88.28]
cc-pV(Q+d)Z	−47.19	−48.82	+7.35	−3.47	[−0.21]	[−0.28]	[−92.62]
Extrapolation	[−47.20]	[−50.82]	[+ 7.47]	[−3.61]	[−0.21]	[−0.28]	[−94.65]

Table 9 Incremented focal point energies in kcal mol^{-1} for terminal P_4O. Total energies are relative to tetrahedral P_4 plus ^{3}P oxygen and are reported as Net/Extrapolation + ΔZPVE

Terminal P_4O							
Total = −84.04 + 2.35 = −81.7 kcal mol^{-1}							
	ΔHF	+δ MP2	+δ CCSD	+δ CCSD(T)	+δ CCSDT	+δ CCSDT(Q)	Net
cc-pV(D+d)Z	−15.28	−52.11	+12.05	−4.15	−0.10	−0.64	[−60.24]
cc-pV(T+d)Z	−28.96	−56.23	+13.50	−5.18	[−0.10]	[−0.64]	[−77.61]
cc-pV(Q+d)Z	−30.32	−59.23	+13.68	−5.39	[−0.10]	[−0.64]	[−82.00]
Extrapolation	[−30.15]	[−61.41]	[+ 13.81]	[−5.55]	[−0.10]	[−0.64]	[−84.04]

Table 10 Incremented focal point energies in kcal mol^{-1} for P_4O_2 (D_{2d}). Total energies are relative to tetrahedral P_4 plus $^3\Sigma_g^-$ O_2 and are reported as Net/Extrapolation +ΔZPVE

P_4O_2 (D_{2d})							
Total = −63.97 + 1.98 = −62.0 kcal mol^{-1}							
	ΔHF	+δ MP2	+δ CCSD	+δ CCSD(T)	+δ CCSDT[a]	+δ CCSDT(Q)[b]	Net
cc-pV(D+d)Z	−43.39	+24.54	−16.74	+1.55	−1.87	+0.78	[−35.12]
cc-pV(T+d)Z	−62.34	+20.88	−18.13	+2.17	[−1.87]	[+0.78]	[−58.52]
cc-pV(Q+d)Z	−64.72	+18.66	−18.54	+2.31	[−1.87]	[+0.78]	[−63.39]
Extrapolation	[−64.76]	[+17.04]	[−18.84]	[+2.41]	[−1.87]	[+0.78]	[−65.25]

[a] DLPNO-CCSDT − CCSD(T). [b] DLPNO-CCSDT(Q) − DLPNO-CCSDT.

nearly equal magnitude (*ca.* 18 kcal mol^{-1}). CCSD(T)/cc-pV(T+d)Z overestimates the net extrapolated energy by about 1 kcal mol^{-1}. For the interested investigator, we provide the energy of $\frac{1}{2}\left[^3\Sigma_g^- O_2\right] \rightarrow {}^3$P oxygen (+58.6 kcal mol^{-1}) using single point energy computations and zero-point vibrational energy contributions at the same levels of theory as used in our focal point analysis for comparison to previously reported P_4O_2 species with optimal error cancellation.[72] The experimental value for $\frac{1}{2}\left[^3\Sigma_g^- O_2\right] \rightarrow {}^3$P oxygen is 59.0 kcal mol^{-1}.[87]

4. Conclusion

Three P_4O species were characterized using the CCSD(T)/cc-pV(T+d)Z method for resolution of existing vibrational and mechanistic discrepancies in the literature. Vibrational bands assigned to C- and T-P_4O by Andrews and coworkers are substantiated, while we believe the symmetric P–O stretch band of B-P_4O assigned to 553 cm^{-1} is instead a previously unassigned 770 cm^{-1} band. The molecular species responsible for the vibrational bands previously assigned to B-P_4O remains elusive, but we predict they do not belong to a D_{2d}-symmetry

P_4O_2 molecule. We found no evidence for a direct isomerization pathway between T- and B-P_4O, instead finding a two-step mechanism proceeding through a P_3-PO intermediate. Our previous vibrational band assignment for the positive combination antisymmetric P–O stretch of cyclic-P_4O_2 has been revised, and we now believe it to be a previously unassigned 919 cm^{-1} band.

Further experimental investigation into these species is encouraged. Current vibrational assignments rely on matrix-isolation spectroscopy, where definitive characterization can be difficult due to the presence of many different species. Mass-selected gas-phase spectroscopy could provide unambiguous identification; however, low production yields may preclude direct absorption measurements. Action-based spectroscopic techniques could circumvent this limitation, necessitating complementary theoretical characterization of charged P_4O species.

Conflicts of interest

There are no conflicts to declare.

Data availability

The data supporting this article has been included as part of the supplementary information (SI). Supplementary information: Tables S1–S4, containing the computed fundamental, harmonic, and isotopic frequencies at the reported levels of theory. Cartesian coordinates for the optimized geometries are also included. See DOI: https://doi.org/10.1039/d6cp00698a.

Acknowledgements

E. J. P and Y. A. acknowledge the Air Force Office of Scientific Research (AFOSR) grant number FA9550-23-1-0375, the Gordon and Betty Moore Foundation, GBMF12246, and partial support from NSF Grant No. 2152159 (NRT-QuaNTRASE). The research of the H. F. S. group is supported by the U.S. Department of Energy, Office of Basic Energy Sciences, Chemical Sciences Division, Fundamental Interactions, Computational and Theoretical Chemistry (CTC) program, contract DE-SC0018412. E. J. P, A. G. H., and M. E. L. thank Dr. Rollin A. King (Bethel University) and Dr. Wesley D. Allen (University of Georgia) for their guidance.

References

1 A. Favron, E. Gaufres, F. Fossard, A.-L. Phaneuf-L'Heureux, N. Y. Tang, P. L. Levesque, A. Loiseau, R. Leonelli, S. Francoeur and R. Martel, Photooxidation and quantum confinement effects in exfoliated black phosphorus, *Nat. Mater.*, 2015, **14**, 826–832.
2 Y. Abate, D. Akinwande, S. Gamage, H. Wang, M. Snure, N. Poudel and S. B. Cronin, Recent progress on stability and passivation of black phosphorus, *Adv. Mater.*, 2018, **30**, 1704749.
3 L. Zhang, H. Huang, B. Zhang, M. Gu, D. Zhao, X. Zhao, L. Li, J. Zhou, K. Wu and Y. Cheng, *et al.*, Structure and properties of violet phosphorus and its phosphorene exfoliation, *Angew. Chem.*, 2020, **132**, 1090–1096.
4 W. Ahmad, A. Abbas, U. Younis, J. Zhang, S. H. Aleithan and Z. Wang, Advancements in optoelectronics: harnessing the potential of 2D violet phosphorus, *Adv. Func. Mater.*, 2024, **34**, 2410723.
5 P. C. Debnath, K. Park and Y.-W. Song, Recent advances in black-phosphorus-based photonics and optoelectronics devices, *Small Methods*, 2018, **2**, 1700315.
6 Y. Huang, J. Qiao, K. He, S. Bliznakov, E. Sutter, X. Chen, D. Luo, F. Meng, D. Su and J. Decker, *et al.*, Interaction of black phosphorus with oxygen and water, *Chem. Mater.*, 2016, **28**, 8330–8339.
7 Q. Li, H. Yang, X. Zheng, Y. Chen, C. Wang, Y. Han, Y. Guo, X. Zheng and Y. Wei, Thinning Effect of Few-Layer Black Phosphorus Exposed to Dry Oxidation, *Nanomaterials*, 2025, **15**, 974.
8 Y. Kaddar, Z. Mansouri, A. Benyoussef, A. El Fatimy and O. Mounkachi, Elucidating the Oxidation Process and Enhanced Stability of Black Phosphorus through NTCDA Passivation: A Molecular Dynamics Study, *Adv. Theory Simul.*, 2025, 2401205.
9 K. L. Kuntz, R. A. Wells, J. Hu, T. Yang, B. Dong, H. Guo, A. H. Woomer, D. L. Druffel, A. Alabanza and D. Tomanek, *et al.*, Control of surface and edge oxidation on phosphorene, *ACS Appl. Mater. Interfaces*, 2017, **9**, 9126–9135.
10 K. L. Utt, P. Rivero, M. Mehboudi, E. O. Harriss, M. F. Borunda, A. A. Pacheco SanJuan and S. Barraza-Lopez, Intrinsic defects, fluctuations of the local shape, and the photo-oxidation of black phosphorus, *ACS Cent. Sci.*, 2015, **1**, 320–327.
11 M. S. Oakley, J. J. Bao, M. Klobukowski, D. G. Truhlar and L. Gagliardi, Multireference Methods for Calculating the Dissociation Enthalpy of Tetrahedral P4 to Two P2, *J. Phys. Chem. A*, 2018, **122**, 5742–5749.
12 L. Andrews and R. Withnall, Matrix Reactions of Oxygen Atoms with P4. Infrared Spectra of P_4O, P_2O, PO, and PO_2, *Cheminform*, 1988, **19**, 5605–5611.
13 M. Ghafariasl, S. Singh, S. Gamage, T. Prusnick, M. Snure and Y. Abate, Photodegradation and Thermal Effects in Violet Phosphorus, *Adv. Mater. Interfaces*, 2024, **11**, 2300794.
14 L. R. Maxwell, S. B. Hendricks and L. S. Deming, The Molecular Structure of P_4O_6, P_4O_8, P_4O_{10} and As_4O_6 by Electron Diffraction, *J. Chem. Phys.*, 1937, **5**, 626–637.
15 A. Chapman, Spectra of phosphorus compounds—III The vibrational assignment and force constants of P4O6 and P4O10. Spectrochim, *Act A Mol. Biomol. Spectrosc.*, 1968, **24**, 1687–1696.
16 B. Beagley, D. W. J. Cruickshank, T. G. Hewitt and K. H. Jost, Molecular structures of P4O6 and P_4O_8, *Trans. Faraday Soc.*, 1969, **65**, 1219–1230.

17 Z. Mielke and L. Andrews, Infrared spectra of phosphorus oxides (P_4O_6, P_4O_7, P_4O_8, P_4O_9 and P_4O_{10}) in solid argon, *J. Phys. Chem.*, 1989, **93**, 2971–2976.
18 R. G. Egdell, M. H. Palmer and R. H. Findlay, Electronic structure of the Group 5 oxides: photoelectron spectra and ab-initio molecular orbital calculations, *Inorg. Chem.*, 1980, **19**, 1314–1319.
19 J. L. Rose, T. C. VanCott, P. N. Schatz, M. E. Boyle and M. H. Palmer, Vacuum ultraviolet spectroscopy of Group V oxides: P_4O_6 and As_4O_6, *J. Phys. Chem.*, 1989, **93**, 3504–3511.
20 L. Andrews, M. McCluskey, Z. Mielke and R. Withnall, Matrix reactions of P4 and P2 with O3 molecules, *J. Mol. Struct.*, 1990, **222**, 95–108.
21 Z. Mielke and L. Andrews, Matrix infrared spectra of the products from photochemical reactions of tetraphosphorus with ozone and decomposition of tetraphosphorus hexoxide, *Inorg. Chem.*, 1990, **29**, 2773–2779.
22 Z. Mielke, M. McCluskey and L. Andrews, Matrix reactions of P2 and O3 molecules, *Chem. Phys. Lett.*, 1990, **165**, 146–154.
23 M. McCluskey and L. Andrews, Matrix infrared spectra of the products of the phosphorus (P2) and ozone reaction, *J. Phys. Chem*, 1991, **95**, 2988–2994.
24 M. McCluskey and L. Andrews, Infrared spectra of products formed by the photoinduced reactions of phosphorus-oxygen ((P2) x (O2) y) clusters in solid argon, *J. Phys. Chem.*, 1991, **95**, 2679–2687.
25 R. C. Mowrey, B. A. Williams and C. H. Douglass, Vibrational Analysis of P_4O_6 and P_4O_{10}, *J. Phys. Chem. A*, 1997, **101**, 5748–5752.
26 C. Bauschlicher, M. Zhou and L. Andrews, A study of the products of the reaction of phosphorus and dioxygen, *J. Phys. Chem. A*, 2000, **104**, 3566–3571.
27 I. R. Beattie, K. M. S. Livingston, G. A. Ozin and D. J. Reynolds, Single-crystal Raman spectra of arsenolite (As_4O_6) and senarmonite (Sb_4O_6). The gas-phase Raman spectra of P4O6, P_4O_{10}, and As_4O_6, *J. Chem. Soc. A*, 1970, 449–451.
28 Y. Wang, Y. Xie, P. Wei, H. F. Schaefer III, P. V. R. Schleyer and G. H. Robinson, Splitting Molecular Oxygen en Route to a Stable Molecule Containing Diphosphorus Tetroxide, *J. Am. Chem. Soc.*, 2013, **135**, 19139–19142.
29 J. S. Francisco, Coupled cluster study of the energetic and spectroscopic properties of OPO x (x= O,+ 1,- 1), *J. Chem. Phys.*, 2002, **117**, 3190–3195.
30 X. Chu, W. Qian, B. Lu, L. Wang, J. Qin, J. Li, G. Rauhut, T. Trabelsi, J. S. Francisco and X. Zeng, The triplet hydroxyl radical complex of phosphorus monoxide, *Angew. Chem.*, 2020, **132**, 22133–22137.
31 L. L. Lohr, An ab initio characterization of the tetraphosphorus oxide P_4O, *J. Phys. Chem.*, 1990, **94**, 4832–4835.
32 L. Yao, Y. Chen and G. Liu, Theoretical study of the oxidation mechanisms of excited P4Ox (x = 1–3) and the anharmonic effect on the main reactions, *Chem. Phys. Lett.*, 2023, **814**, 140328.
33 J. F. Stanton, Why CCSD(T) works: a different perspective, *Chem. Phys. Lett.*, 1997, **281**, 130–134.
34 B. P. Pritchard, D. Altarawy, B. Didier, T. D. Gibsom and T. L. Windus, A New Basis Set Exchange: An Open, Up-to-date Resource for the Molecular Sciences Community, *J. Chem. Inf. Model.*, 2019, **59**, 4814–4820.
35 D. Feller, The role of databases in support of computational chemistry calculations, *J. Comput. Chem.*, 1996, **17**, 1571–1586.
36 K. L. Schuchardt, B. T. Didier, T. Elsethagen, L. Sun, V. Gurumoorthi, J. Chase, J. Li and T. L. Windus, Basis Set Exchange: A Community Database for Computational Sciences, *J. Chem. Inf. Model.*, 2007, **47**, 1045–1052.
37 T. H. Dunning, Gaussian basis sets for use in correlated molecular calculations. I. The atoms boron through neon and hydrogen, *J. Chem. Phys.*, 1989, **90**, 1007–1023.
38 T. H. Dunning, K. A. Peterson and A. K. Wilson, Gaussian basis sets for use in correlated molecular calculations. X. The atoms aluminum through argon revisited, *J. Chem. Phys.*, 2001, **114**, 9244–9253.
39 D. E. Woon and T. H. Dunning, Gaussian basis sets for use in correlated molecular calculations. III. The atoms aluminium through argon, *J. Chem. Phys.*, 1993, **98**, 1358–1371.
40 I. Mills, *Vibration-rotation structure in asymmetric and symmetric top molecules*, 1972.
41 P. R. Franke, J. F. Stanton and G. E. Douberly, How to VPT2: Accurate and Intuitive Simulations of CH Stretching Infrared Spectra Using VPT2 + K with Large Effective Hamiltonian Resonance Treatments, *J. Phys. Chem. A*, 2021, **125**, 1301–1324.
42 A. D. Becke, Density-functional thermochemistry. III. The role of exact exchange, *J. Chem. Phys.*, 1993, **98**, 5648–5652.
43 C. Lee, W. Yang and R. G. Parr, Development of the Colle-Salvetti correlation-energy formula into a functional of the electron density, *Phys. Rev. B*, 1988, **37**, 785–789.
44 S. H. Vosko, L. Wilk and M. Nusair, Accurate spin-dependent electron liquid correlation energies for local spin density calculations: a critical analysis, *Can. J. Phys.*, 1980, **58**, 1200–1211.
45 P. J. Stephens, F. J. Devlin, C. F. Chabalowski and M. J. Frisch, Ab initio calculation of vibrational absorption and circular dichroism spectra using density functional force fields, *J. Phys. Chem.*, 1994, **98**, 11623–11627.
46 M. Hochlaf, C. Puzzarini and M. L. Senet, Towards the computations of accurate spectroscopic parameters and vibrational spectra for organic compounds, *Mol. Phys.*, 2015, **113**, 1661–1673.
47 C. Levi, J. M. Martin and I. Bar, Fundamental vibrational frequencies and dominant resonances in methylamine isotopologues by ab initio and density functional theory methods, *J. Comput. Chem.*, 2008, **29**, 1268–1276.
48 R. P. Bettens, Comparison of fundamental and harmonic frequencies of first-row closed-shell diatomics calculated using full ab initio methods and composite methods, *J. Phys. Chem. A*, 2004, **108**, 1826–1829.
49 J. C. Howard and G. S. Tschumper, Benchmark structures and harmonic vibrational frequencies near the CCSD (T) complete basis set limit for small water clusters:(H2O) n= 2, 3, 4, 5, 6, *J. Chem. Theory Comput.*, 2015, **11**, 2126–2136.

50 Y. Fang, F. Liu, S. J. Klippenstein and M. I. Lester, Direct observation of unimolecular decay of CH3CH2CHOO Criegee intermediates to OH radical products, *J. Chem. Phys.*, 2016, 145.

51 S. J. Klippenstein, C. R. Mulvihill and P. Glarborg, Theoretical kinetics predictions for reactions on the NH2O potential energy surface, *J. Phys. Chem. A*, 2023, **127**, 8650–8662.

52 A. G. Csaszar, W. D. Allen and H. F. Schaefer III, In pursuit of the ab initio limit for conformational energy prototypes, *J. Chem. Phys.*, 1998, **108**, 9751–9764.

53 M. S. Schuurman, S. R. Muir, W. D. Allen and H. F. Schaefer III, Toward subchemical accuracy in computational thermochemistry: Focal point analysis of the heat of formation of NCO and [H,N,C,O] isomers, *J. Chem. Phys.*, 2004, **120**, 11586–11599.

54 D. Feller, The use of systematic sequences of wave functions for estimating the complete basis set, full configuration interaction limit in water, *J. Chem. Phys.*, 1993, **98**, 7059–7071.

55 T. Helgaker, W. Klopper, H. Koch and J. Noga, Basis-set convergence of correlated calculations on water, *J. Chem. Phys.*, 1997, **106**, 9639–9646.

56 J. Noga and R. J. Bartlett, The full CCSDT model for molecular electronic structure, *J. Chem. Phys.*, 1987, **86**, 7041–7050.

57 Y. J. Bomble, J. F. Stanton, M. Kallay and J. Gauss, Coupled-cluster methods including noniterative corrections for quadruple excitations, *J. Chem. Phys.*, 2007, **123**, 054101.

58 A. Jiang, Z. L. Glick, D. Poole, J. M. Turney, C. D. Sherrill and H. F. Schaefer III, Accurate and efficient open-source implementation of domain-based local pair natural orbital (DLPNO) coupled-cluster theory using a t1-transformed Hamiltonian, *J. Chem. Phys.*, 2024, 161.

59 A. Jiang, H. F. Schaefer III and J. M. Turney, Linear-Scaling Local Natural Orbital-Based Full Triples Treatment in Coupled-Cluster Theory, *J. Chem. Theory Comput.*, 2025, **21**, 2386–2401.

60 A. Jiang, H. F. Schaefer III and J. M. Turney, Linear-scaling quadruple excitations in local pair natural orbital coupledcluster theory, *J. Chem. Phys.*, 2025, 162.

61 H.-J. Werner, P. J. Knowles, G. Knizia, F. R. Manby and M. Schutz, Molpro: a general-purpose quantum chemistry program package, *WIREs Comput. Mol. Sci.*, 2012, **2**, 242–253.

62 H.-J. Werner, P. J. Knowles, F. R. Manby, J. A. Black, K. Doll, A. Hesselman, D. Kats, A. Kohn, T. Korona and D. A. Kreplin, *et al.*, The Molpro quantum chemistry package, *J. Chem. Phys.*, 2020, **152**, 144107.

63 H.-J. Werner, P. J. Knowles, P. Celani, W. Gyorffy, A. Hesselman, D. Kats, G. Knizia, A. Kohn, T. Korona, D. Kreplin, *et al.*, *MOLPRO, version 2022.1*, a package of ab initio programs.

64 F. Neese, The ORCA program system, *Wiley Interdiscip. Rev.: Comput. Mol. Sci.*, 2012, **2**, 73–78.

65 F. Neese, An improvement of the resolution of the identity approximation for the formation of the Coulomb matrix, *J. Comput. Chem.*, 2003, **24**, 1740–1747.

66 F. Neese, F. Wennmohs, A. Hansen and U. Becker, Efficient, approximate and parallel Hartree–Fock and hybrid DFT calculations. A 'chain-of-spheres' algorithm for the Hartree–Fock exchange, *Chem. Phys.*, 2009, **356**, 98–109.

67 S. Grimme, J. Antony, S. Ehrlich and H. Krieg, A Consistent and Accurate Ab Initio Parametrization of Density Functional Dispersion Correction (DFT-D) for the 94 Elements H-Pu, *J. Chem. Phys.*, 2010, **132**, 154104.

68 S. Grimme, S. Ehrlich and L. Goerigk, Effect of the damping function in dispersion corrected density functional theory, *J. Comput. Chem.*, 2011, **32**, 1456–1465.

69 D. G. A. Smith, *et al.*, Psi4 1.4: Open-Source Software for High-Throughput Quantum Chemistry, *J. Chem. Phys.*, 2020, **152**(18), 184108.

70 D. Mester, P. R. Nagy, J. Csoka, L. Gyevi-Nagy, P. B. Szabo, R. A. Horvath, K. Petrov, B. Hegely, B. Ladoczki and G. Samu, *et al.*, Overview of developments in the MRCC program system, *J. Phys. Chem. A*, 2025, **129**, 2086–2107.

71 M. Kallay, P. Nagy, D. Mester, L. Gyevi-Nagy, J. Csoka, P. Szabo, Z. Rolik, G. Samu, J. Csontos and B. Hegely, *et al.*, Mrcc, a quantum chemical program suite written by, *J. Chem. Phys*, 2020, **152**, 17407.

72 E. J. Poncelet, M. E. Lahm, A. G. Poncelet, J. M. Turney, M. A. Duncan, H. F. Schaefer III and Y. Abate, Vibrational Signatures of Unrealized Phosphorus Suboxide Intermediates in White Phosphorus Oxidation Reactions, *J. Phys. Chem. A*, 2026, **130**, 121–128.

73 P. R. Schreiner, H. P. Reisenauer, D. Ley, D. Gerbig, C.-H. Wu and W. D. Allen, Methylhydroxycarbene: Tunneling Control of a Chemical Reaction, *Science*, 2011, **332**, 1300–1303.

74 B. Myer, *Low Temperature Spectroscopy: Optical Properties of Molecules in Matrices, Mixed Crystals, and Frozen Solutions*, American Elsevier Publishing Company, 1971.

75 S. Bailleux, M. Bogey, C. Demuynck, Y. Liu and A. Walters, Millimeter-wave spectroscopy of PO in excited vibrational states up to v= 7, *J. Mol. Spectrosc.*, 2002, **216**, 465–471.

76 B. M. Cossairt, C. C. Cummins, A. R. Head, D. L. Lichtenberger, R. J. F. Berger, S. A. Hayes, N. W. Mitzel and G. Wu, On the Molecular and Electronic Structures of As P_3 and P_4, *J. Am. Chem. Soc.*, 2010, **132**, 84598465.

77 W. D. Allen and A. G. Csaszar, On the ab initio determination of higher-order force constants at nonstationary reference geometries, *J. Chem. Phys.*, 1993, **98**, 2983–3015.

78 F. Paw Lowski, A. Halkier, P. Jorgensen, K. L. Bak, T. Helgaker and W. Klopper, Accuracy of spectroscopic constants of diatomic molecules from ab initio calculations, *J. Chem. Phys.*, 2003, **118**, 2539–2549.

79 M. E. Lahm, N. L. Kitzmiller, H. F. Mull, W. D. Allen and H. F. Schaefer III, Concordant Mode Approach for Molecular Vibrations, *J. Am. Chem. Soc.*, 2022, **144**, 23271–23274.

80 N. L. Kitzmiller, M. E. Lahm, L. N. Olive Dornshuld, J. Jin, W. D. Allen and H. F. Schaefer III, Convergent Concordant Mode Approach for Molecular Vibrations: CMA-2, *J. Chem. Theory Comput.*, 2024, **20**, 10886–10898.

81 L. N. O. Dornshuld, M. E. Lahm, N. L. Kitzmiller, W. D. Allen and H. F. Schaefer III, Concordant Mode Approach (CMA): Vibrational Analysis of New and Upgraded Intermolecular Benchmarks for Noncovalent Bonding, *J. Phys. Chem. A*, 2026, **130**, 3249–3260.
82 W. D. Allen, A. G. Csaszar and D. A. Horner, The puckering inversion barrier and vibrational spectrum of cyclopentene. A scaled quantum mechanical force field algorithm, *J. Am. Chem. Soc.*, 1992, **114**, 6834–6849.
83 P. Pulay and F. Torok, Uber die Parameterdarstellung der Kraftkonstantenmatrix, *I. Acta Chim. Hung*, 1965, **44**, 287.
84 G. Keresztury and G. Jalsovszky, An alternative calculation of the vibrational potential energy distribution, *J. Mol. Struct.*, 1971, **10**, 304–305.
85 D. Peng and M. Reiher, Exact decoupling of the relativistic Fock operator, *Theor. Chem. Acc.*, 2012, **131**, 1081.
86 W. Liu and D. Peng, Exact two-component Hamiltonians revisited, *J. Chem. Phys.*, 2009, 131.
87 P. Wang, S. Gong and Y. Mo, Bond dissociation energy of O_2 measured by fully state-to-state resolved threshold fragment yield spectra, *J. Chem. Phys.*, 2024, **160**, 164302.